Two-dimensional granular flow in a small-angle funnel

C. T. Veje and P. Dimon
The Center for Chaos and Turbulence Studies, The Niels Bohr Institute, Blegdamsvej 17, DK-2100 Copenhagen Ø, Denmark
(Received 15 March 1996)

We have investigated a granular flow consisting of a single layer of uniform balls in a two dimensional funnel. The qualitative behavior of the flow depends in a sensitive way on the geometry. For a particular configuration in which only the funnel opening angle β is varied, we find three regimes. When $\beta > 2°$, the flow is dense and steady, and the flow rate is determined by the geometry at the outlet. When $0.1° \lesssim \beta \lesssim 1°$, the flow is intermittent, consisting of quasiperiodic kinematic waves, probably shock waves, propagating against the flow. The flow rate reaches its maximum in this regime. When $\beta < 0.05°$, the waves become stationary, and the flow rate is now determined by the geometry at the inlet. We also measure the number density fluctuations of the flow and their power spectra. For all flows, the power spectra are white at low frequencies with structures at higher frequencies resulting from the kinematic waves and short-range correlations. [S1063-651X(96)02510-X]

PACS number(s): 46.10.+z, 83.70.Fn, 05.40.+j

I. INTRODUCTION

The properties of granular matter are as varied as they are unusual. (For reviews and recent developments, see, for example, Refs. [1–7].) In particular, granular flows differ in many respects from hydrodynamic flows. It is known, for example, that the flow rate in an hourglass is essentially independent of the head of the granular material [8]. Furthermore, the flow is not necessarily steady, for example, there can be fluctuations in the flow rate.

In this paper we have examined the flow properties of a single layer of uniform balls rolling down an inclined plane through a two-dimensional funnel [9]. It is therefore a two dimensional analog of an hourglass, but with the capability to actually observe details of the flow. We measure average flow rates and also number density fluctuations and their power spectra.

Previous experimental studies of granular flows have mostly concentrated on measuring steady-state properties of stresses and flow velocities [10], and density profiles [11]. Dynamic studies are less common. Density waves have been observed in wide-angle hoppers [1,12]. Dynamic measurements have been made of the density fluctuations of sand in an hourglass by Schick and Verveen [13]. They found density waves in the form of ''slugs'' whose power spectrum yielded an apparent $1/f$ region. This experiment was the motivation for the present work, although, as will be shown later, we find no $1/f$ noise. (We have also repeated the hourglass experiment and suggest a simpler interpretation of the power spectrum [14].) More recently, Wu *et al.* [15] have studied the flow rate fluctuations in an hourglass and have observed a periodic ''ticking'' when there is a counterflow of air.

Theoretically, a wide variety of methods including plasticity theory [2], hydrodynamics [16], soil mechanics [17], kinetic gas theory [18], and statistical mechanics [19] have been applied to granular matter. However, these tend to target only certain aspects of the observed phenomena, and there is as yet no comprehensive theory. Computer simulations have been performed using molecular dynamics (MD) [20,21], lattice gas automata (LGA) [22], and cellular automata [23]. Both the MD and LGA simulations have found density waves in the flow. In particular, the LGA simulations of flow in a pipe [22] produced kinematic waves with $1/f$ noise in the power spectrum of the density fluctuations, although only for special values of injection rates or average densities. Nevertheless, the presence of dissipation and boundary roughness were found to be of paramount importance in generating kinematic waves. (We have also been informed that when friction was turned off completely in MD simulations, there were no kinematic waves [24].)

The paper is organized as follows. In Sec. II we describe the experimental setup. In Sec. III we discuss the qualitative behavior of the flow, and present the number density fluctuation measurements and their power spectra. The flow rate measurements are described in Sec. IV, and finally Sec. V contains a summary of the work.

II. EXPERIMENT

The granular material was composed of 3.175 mm diameter brass balls (0.2% sphericity) of mass 0.14 g. Brass was necessary to avoid problems caused by the slow magnetization of steel balls. Approximately 50 000 balls were used in the experiment. When piled, their angle of repose was determined to be $\sim 15°$.

The experimental setup is shown in Fig. 1(a). Two aluminum walls (A) of height 3.2 mm (slightly greater than one ball diameter) rested on a 3 m long transparent acrylic plane (B). The walls had a 2 m long straight section which then curved smoothly at the top (50 cm radius of curvature) to form a reservoir area (C). They could be adjusted so as to vary the geometry of the funnel and were grounded to discharge static electricity carried by the balls. A second transparent covering sheet (not shown) was placed on top of the walls. (This was necessary since the kinematic waves which we will discuss later could be sufficiently violent to kick balls out of the funnel.) The plane (B) was mounted to a table at one end by a rotating joint (D) so its incline could be adjusted with a jack (E).

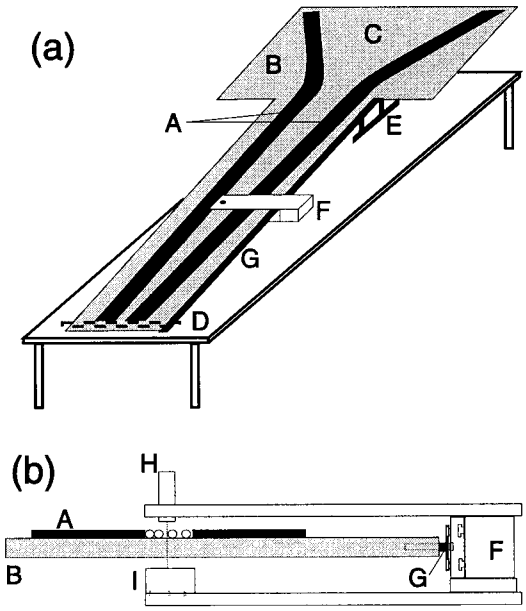

FIG. 1. (a) The experimental setup. (b) A number density measuring device (see text).

A device for measuring the local number density, shown in detail in Fig. 1(b), consisted of a slide (F) mounted on a rail (G) so that it could be positioned anywhere along the funnel. A 1 mW 670 nm laser diode (H) and a photodiode (I) were mounted on the slide so that the beam passed through the plane (B). The beam was focused in the plane of the balls forming a spot $\sim 1\%$ of the cross-sectional area of a ball. This is effectively a point measurement and the photodiode output was either low or high depending on whether there was a ball in the beam or not. All measurements were made along the center line of the funnel. (We also made measurements using a 1 mm wide line detector which covered the width of the funnel, but this was technically cumbersome and yielded essentially the same results.) The detector was light shielded as a precaution, although the signal-to-noise ratio was not a problem. The signal from the photodiode was measured with a HP3562A Dynamic Signal Analyzer. The frequency response of the photodiode is nominally flat up to ~ 10 kHz, but we never measured beyond 1 kHz.

A top view schematic of the geometry of the funnel is shown in Fig. 2 (with the exception of the inclination angle). There were three independent flow parameters which were varied in the following ranges: opening angle β (0°–4°), outlet width D (0–30 mm), and inclination angle θ (0°–5°). The detector position x was measured from the outlet. The other parameters in the figure will be discussed later.

At the beginning of a run, the outlet was blocked, and the balls were poured onto the reservoir area and allowed to fill the system. After a short transient period, the behavior of the flow was independent of the initial configuration of the balls in the reservoir, whether random or close packed, or simply left in a pile, which was by far the most convenient. (Since the angle of inclination was always far below the angle of repose, the balls would form a two-dimensional layer well before entering the funnel.) Flow rates varied between ~ 50 and 500 balls/s, so a single run with 50 000 balls lasted 100–1000 s accordingly. In most cases, to obtain longer runs and hence better averages, the balls were recycled by pouring them back onto the reservoir area in such a way that the flow was not visibly disturbed.

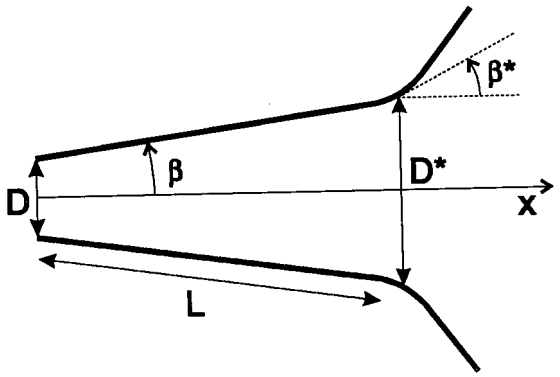

FIG. 2. A schematic top view of the funnel showing the geometry.

Interstitial fluid effects

The Bagnold number measures the ratio of the viscous drag on an object to its weight, and hence the importance of the effect of the interstitial fluid on the granular flow. For laminar flow around a (nonrotating) sphere of radius a and mass m, $\mathrm{Ba}=6\pi\eta\overline{v}a/mg$ where η is the dynamic viscosity of the fluid, $\overline{v}$ is the mean relative velocity, and g is the gravitational acceleration. In our experiment, the largest velocity a ball can achieve (i.e., rolling freely down the plane) is ~ 100 cm/s, so with $\eta = 1.7\times 10^{-4}$ g/cm s for air, Ba $\sim 10^{-4}$, which would suggest that viscous drag is an unimportant effect. However, strong collective effects can appear for sand flow in an hourglass even though the Bagnold number is small [15]. We do not encounter these effects since our system is not sealed and there is no counterflow of air.

We must also consider if the interstitial fluid flow is, in fact, laminar, since turbulence can significantly increase the viscous drag. Using the numbers given above, and the kinematic viscosity for air $\nu = 0.13$ cm^2/s, we obtain a Reynold's number $\mathrm{Re}=2a\overline{v}/\nu \approx 130$. Boundary layer separation, time dependent flow, and turbulence occur at Re ≈ 25, 130, and 200, respectively [25], so for our worst-case estimate, we may be nearing a regime where turbulence will have some effect on the flow.

III. GENERAL BEHAVIOR

A well-known property of the flow of granular material through apertures is the existence of stagnant regions [1]. All flow occurs in a pseudofunnel with an opening angle β_c called the angle of approach. For example, for steel balls in two dimensions, $\beta_c \approx 15°$ [1]. In the present experiment, we are always well below the angle of approach so there is never a stagnant region. The position of the free-fall arch, the radius at which the balls flow freely and no longer engage in collective behavior, is given by $R_0 = (D-k)/2\sin\beta_c$ where k is the statistically empty space correction [1]. If $\beta < \beta_c$, then k is small, and the free-fall arch occurs at the physical end of the funnel, i.e., $R_0 = D/2\sin\beta$. [However, we have found that at very small angles ($\beta < 1°$) fluctuations become

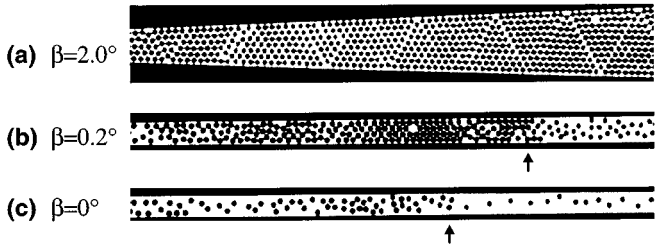

FIG. 3. Snapshot video pictures of the flow with $D=10$ mm and $\theta=4.1°$. The system is illuminated from below. Each picture is 25 cm long with its center at $x=20$ cm. The flow is from right to left. (a) Steady flow. The balls form a triangular lattice with white shear lines between triangular crystallites. (b) Intermittent flow. There is a shock front (arrow) moving to the right against the flow. (c) Pipe flow. In the center is a stationary (but fluctuating) shock front (arrow).

important and the free-fall arch is no longer well defined.]

The fundamental property of dilatancy, formulated by Reynolds [26], is still conceptually important to the understanding of granular flows. It simply states that a granular material must expand in order to flow. In particular, this will result in large density gradients near an aperture which may create density waves [1]. If the granular material is treated as a continuum, it is possible to show that there will be two types of density waves: kinematic (mass transport) and dynamic (sound) [20,27]. In this work, we only observe and measure kinematic waves.

We will now describe the general behavior of the flow. Since it appeared that the funnel opening angle β (see Fig. 2) had the strongest effect, we will use it to parametrize the different flow regimes, although the actual values will, of course, depend on the particular configuration. For the rest of this section, we consider a configuration where the other parameters were fixed at $D=10$ mm and $\theta=4.1°$. The position of the detector was $x=20$ cm unless stated otherwise.

A. Steady flow: $\beta>2°$

In this regime the flow is quite dense, as may be seen in a snapshot video picture in Fig. 3(a). Hence, since the balls are monodisperse, they tend to arrange in a triangular lattice and always such that a primitive lattice vector is parallel to one of the walls. Locally, this structure has the maximum packing fraction in two dimensions $C_{\max}=\pi/2\sqrt{3}\cong 0.91$. As the funnel narrows, however, the triangular lattice must necessarily rearrange itself, forming the white shear lines and the triangular crystallites observable in the figure. The balls appear to mostly roll, but since they are in close contact, they must necessarily slide against each other.

As discussed earlier, dilatant fluctuations are, in fact, observed at the aperture, i.e., the outlet, of the funnel. They appear to occur nearly periodically, which may be a consequence of the periodicity of the shear lines, although it is possible that they are inherently periodic. However, these fluctuations are rather weak, and the flow is essentially steady. We also note that in this regime, the flow rate is completely determined by the geometry at the outlet, e.g., the outlet width D. Neither the geometry at the inlet to the straight section nor the length of the funnel affect the flow rate.

The features just discussed are evident in the number density measurements and their power spectra. The raw signal $V(t)$ from the photodiode (which is linearly related to the number density) is shown for this regime in Fig. 4(a). Due to the high density, the beam is mostly blocked. A composite power spectrum of this signal is shown in Fig. 5(a). The spectrum is white at low frequencies with some structures at higher frequency and finally a rolloff. The rolloff reflects the shape function of an individual ball. This is clear if we compute the mean velocity $\overline{v(x)}$ of a ball at the measuring position x. The number flow rate is $Q=n\overline{v(x)}\mathcal{D}(x)$ where n is the mean number density, and $\mathcal{D}(x)\cong D+2x\beta$ is the width of the funnel at the measuring point. The mean number density can be written as $n=C/\pi a^2$ where C is the packing fraction. Thus, for a typical flow rate of $Q=150$ balls/s, and $C=C_{\max}$, we find that at $x=20$ cm, $\overline{v}\approx 5.5$ cm/s. The frequency associated with a single ball is then $\overline{v}/2a\approx 20$ Hz, which is approximately where the rolloff occurs.

The small peak at ~ 0.5 Hz is attributed to the nearly periodic dilatant fluctuations produced at the outlet. The larger peaks are due to the shear lines. The distance $\Delta(x)$ between the shear lines is found approximately from the geometry to be $\Delta(x)\cong\mathcal{D}(x)/\sqrt{3}\approx 1.4$ cm at $x=20$ cm. This results in a periodicity at $\overline{v}/\Delta\approx 4.0$ Hz which is the peak indicated by the arrow in Fig. 5(a). The peaks at higher frequencies are its harmonics. (There is also a weak peak at ~ 2 Hz which would be the actual periodicity of the shear lines if one took their orientation into account. However, since we are making a point measurement, it is only weakly sensitive to the orientation.) There are no peaks from the close packed triangular lattice of the balls since the lattice crosses the light beam at an angle which depends on β and hence never through a lattice vector (except for special values of β).

Although the detailed shape of a spectrum depends on the measuring position x, it is not qualitatively affected by varying it. For example, at larger x the distance between shear lines increases and the mean flow velocity decreases, hence the corresponding peak positions shift to lower frequencies.

B. Intermittent flow: $0.1°\lesssim\beta\lesssim 1°$

Below $\beta\sim 1°$ the small dilatant fluctuations observed in the steady flow regime form kinematic waves which propagate against the flow. At $\beta=1°$ they tend to decay rapidly, but by $\beta=0.2°$ they propagate the whole length of the funnel, only decaying in the reservoir. These are easily visible by eye and appear as rather local high-density packets shooting upstream at about 1 m/s. They also appear to be produced at roughly 1 s intervals. Consequently, usually no more than 2–3 packets can be seen in the system at one time. As β is decreased further, the nature of the shock waves seems to change. When $\beta\sim 0.1°$, they can be produced anywhere in the funnel. The mechanism for producing them no longer seems to be the dilatant fluctuations at the outlet, but rather the interactions of the balls with the boundaries of the funnel, and with each other. Interestingly enough, the flow rate reaches its maximum in this flow regime at $\beta\sim 0.5°$. We will discuss this later in Sec. IVA.

A video snapshot of a packet is shown in Fig. 3(b) for $\beta=0.2°$. At the left, one observes the density slowly build-

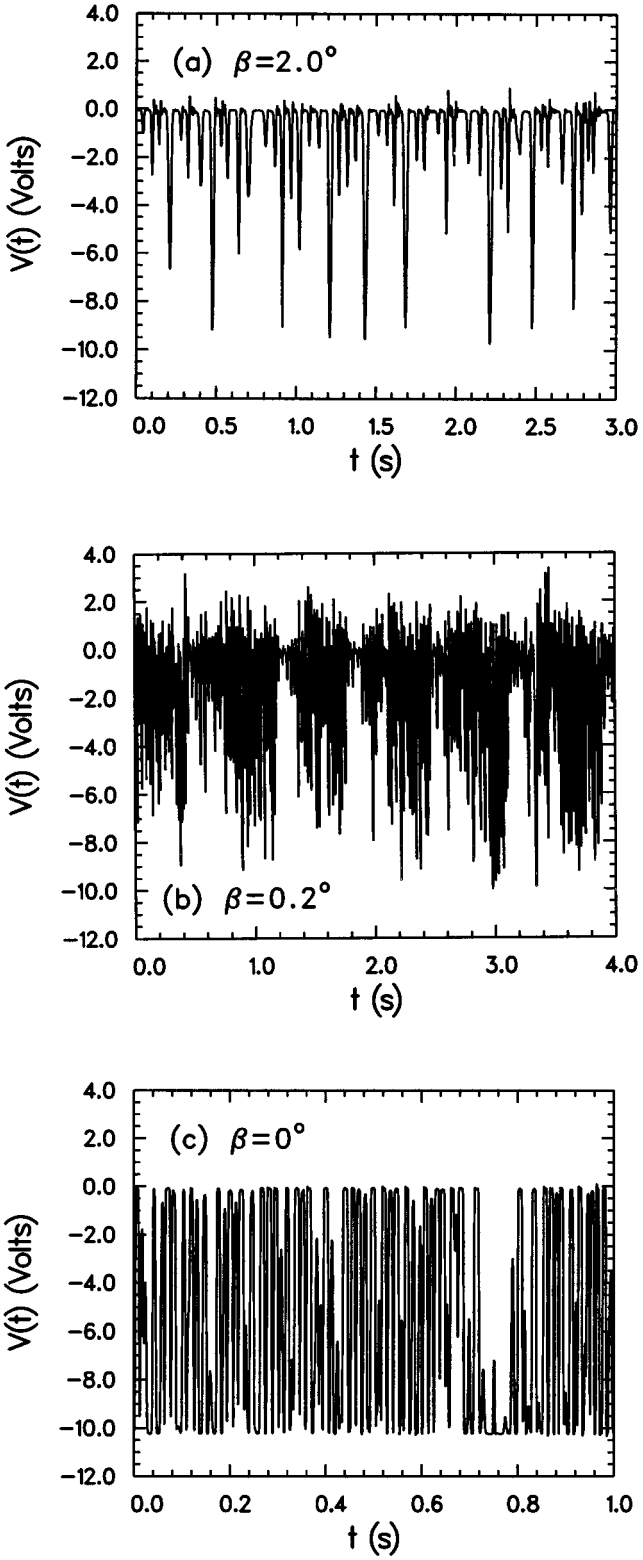

FIG. 4. The raw time signal from the photodiode, sampled at frequency f_s, for the different regimes. A high level (0 V) indicates that the beam is blocked. The signals have been Nyquist filtered which results in some ringing in (a) and (b). (a) Steady flow ($f_s = 200$ Hz). The flow is dense and the beam is mostly blocked. (b) Intermittent flow ($f_s = 200$ Hz). High-density shock waves block the beam in an apparently periodic manner. (c) Pipe flow ($f_s = 2$ kHz). The passage of individual balls can be observed.

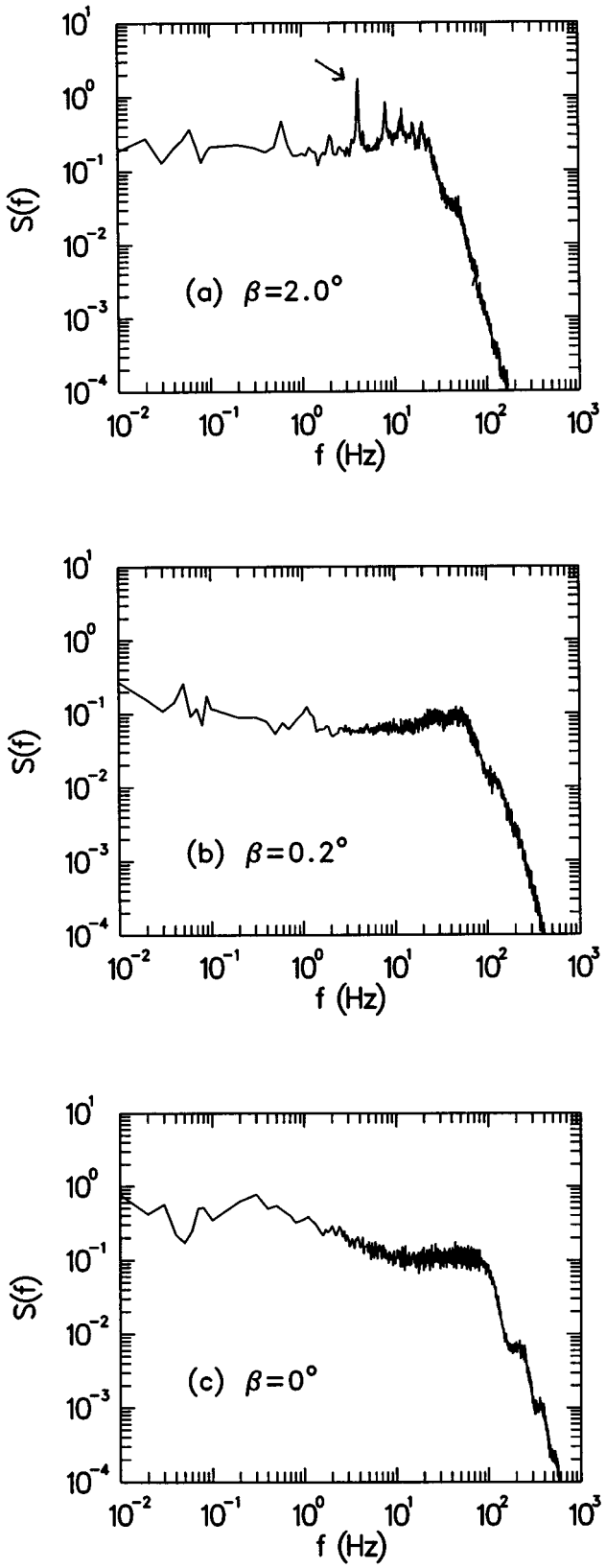

FIG. 5. Composite power spectra in the different flow regimes. The spectra consist of three separate measurements: 0–0.1 Hz (10 averages), 0.1–80 Hz (200 averages), and 80–800 Hz (200 averages). Structures below 0.1 Hz are not statistically significant. (a) Steady flow. The arrow indicates the peak from the periodic shear lines. (b) Intermittent flow. The weak peak at ~ 1 Hz is from the quasiperiodic shock waves. (c) Pipe flow.

ing up to a short, nearly close packed region, then dropping rather abruptly (arrow) to a much lower-density region. This strongly resembles the profile expected for a kinematic shock wave with some broadening due to dissipation [27]. This is not surprising since it is well known that under some very general conditions kinematic waves will evolve into shock waves that may propagate against the flow [27]. In the low-density region the balls both roll freely and slide when they collide. They do not noticeably bounce backward, even at the shock front.

We can roughly estimate the expected shock wave velocity from the available data. A kinematic shock wave travels with velocity $u=(n_2v_2-n_1v_1)/(n_2-n_1)$ where $n_{1,2}$ and $v_{1,2}$ are the mean number densities and velocities to the right (1) and left (2) of the shock front (arrow) in Fig. 3(b) [27]. From the figure, we find that $n_2/n_1\approx 2$. From observing the pulse widths for individual balls in the low-density region, we estimate that $v_1\approx 50$ cm/s. (The mean ball velocity at $x=20$ cm, deduced from the flow rate as in Sec. III A, is $\lesssim 35$ cm/s.) Since the balls are observed to momentarily stop at the shock front, we will suppose that $v_2\approx 0$ (or at least that $v_2/v_1\ll n_1/n_2$). Thus we predict that $u\approx -50$ cm/s where the sign indicates that the shock wave moves in the direction opposite the flow. This is consistent with our measurements which we show later in Sec. III D.

A raw signal measured in the intermittent flow regime is shown in Fig. 4(b). The short blocked regions are a consequence of the short, high-density shock waves. As was observed by eye, these appear to occur almost periodically with a period of ~ 0.8 s. A composite power spectrum is shown in Fig. 5(b). Again, the spectrum is white at low frequencies. The small, broad peak at ~ 1 Hz indicates that the shock waves are not really periodic, but are only weakly quasiperiodic. (This peak is statistically significant and reproducible.) The width of the peak reflects the coherence time of the local periodicity observed in Fig. 4(b). We roughly estimate the coherence time to be ~ 2 s, which is only about twice the apparent period and is why the peak is so weak in the first place. The peak at ~ 60 Hz is due to the noticeable order of the balls along the flow direction as they leave the shock region.

As discussed in the preceding section, the spectra may depend on the measuring position x. In Fig. 6, we compare the spectrum shown in Fig. 5(b) measured at $x=20$ cm with another measured at $x=50$ cm. They are qualitatively similar. In particular, the peak from the quasiperiodic shock waves can still be seen.

C. Pipe flow: $\beta < 0.05°$

At this point, the funnel is effectively a parallel pipe. (In fact, the angle subtended by a ball radius over the length of the funnel is 0.045°.) The shock waves are now stationary, the one farthest upstream ~ 20–30 cm from the reservoir, with the rest nearly evenly spaced downstream ~ 40 cm apart. (Their positions, however, fluctuate as much as ± 10 cm during a run.) Figure 3(c) shows a snapshot of a single shock region. The balls roll more or less freely between shock waves until they collide with a shock front (arrow).

The mechanism that now generates the shock waves is somewhat different than in the intermittent flow regime.

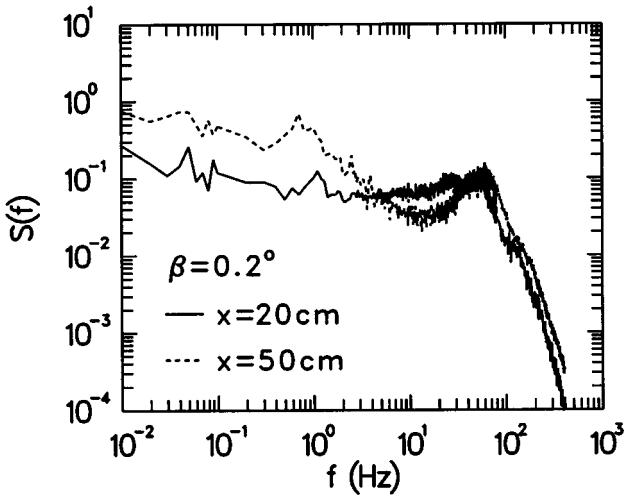

FIG. 6. Dependence of the power spectrum on the measuring position.

When balls enter the pipe from the reservoir, at first they roll freely, accelerating down the incline. It would appear that when they reach a certain velocity, they experience a serious interaction with the covering sheet, slowing them down dramatically. Immediately, balls from behind back up and form a jam. As balls leave the jam, they repeat this process, accounting for the nearly equally spaced positions of the shock waves. When the covering sheet was removed, no jams were observed at all. This demonstrates the importance of roughness and friction in the formation of shock waves as already noted in computer simulations [22].

In the pipe flow regime, the flow rate is completely determined by the geometry at the inlet, since, once a ball leaves the reservoir, it never again interacts with it. For example, the outlet width D no longer plays any role in the flow rate. This should be contrasted with the reverse situation found in the steady flow regime. Also, the length of the funnel is again irrelevant as far as the flow rate is concerned. Thus it would appear that the interesting dynamics, that is, the dynamics that determine the flow rate, move from the outlet to the inlet as β is decreased. Presumably in the intermittent regime, the overall geometry is important since the shock waves can propagate the length of the system, communicating information back upstream. In the pipe flow regime, information cannot be transmitted upstream.

A raw signal measured in the pipe flow regime is shown in Fig. 4(c). One can easily distinguish now the passing of individual balls. A composite power spectrum is shown in Fig. 5(c). There is some weak structure between 100 mHz and 10 Hz which we attribute to the fluctuations of the stationary shock waves through the measuring point. At high frequencies, one can see the details of the shape function of an individual ball.

D. Spatial correlations

Spatial correlations in the flow were measured by using two measuring devices and computing the cross-correlation function $C(x,\ell,\tau)=\overline{V(x+\ell,t+\tau)V(x,t)}$ where ℓ is the separation of the two measuring points and the bar denotes a time average. (This function will depend on x since the sys-

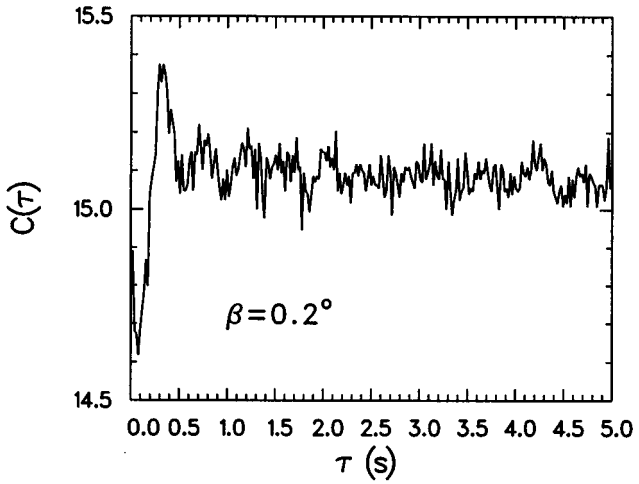

FIG. 7. Cross-correlation function for an intermittent flow with $D=10$ mm, $\theta=4.1°$, $x=50$ cm, and $\ell=20$ cm. The first peak is the time lag τ_1 of a shock wave.

tem lacks translational invariance.) A measurement of $C(x,\ell,\tau)$ is shown in Fig. 7 for an intermittent flow with the same configuration as in Sec. III B with $x=50$ cm and $\ell=20$ cm. The peak at $\tau\sim0.3$ s is due to the correlations caused by the passage of a shock wave, i.e., it is the time lag of a shock wave as it passes from one measuring point to the next. (Some weak oscillations are also visible near the harmonics of this peak since the shock waves are quasiperiodic.) Figure 8 shows the position of this peak τ_1 as a function of the separation ℓ. The dashed line is a linear fit $\tau_1=\ell/v_s$ yielding a mean shock wave velocity $v_s\approx70$ cm/s which is consistent with observations and with the estimate in Sec. III B. (It should be pointed out, however, that the shock wave velocity is almost certainly not constant as it propagates.) The dip before the peak indicates that when a shock wave is produced, it represses for a short time $\lesssim0.2$ s the production of another, i.e., there is a minimum distance between shock waves of ~14 cm. This seems reasonable since it is probably

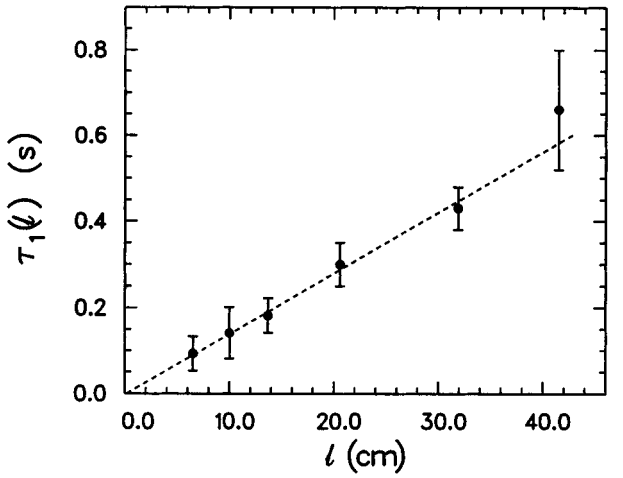

FIG. 8. Position of the first peak in the cross-correlation function as a function of the separation. The inverse of the slope is the shock wave velocity.

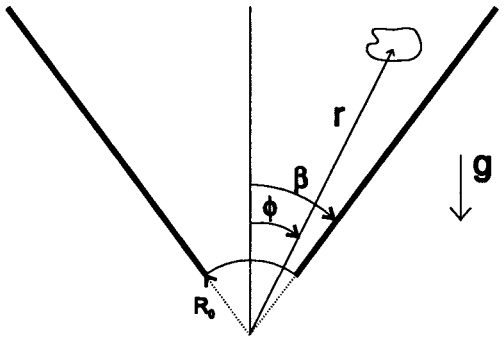

FIG. 9. Geometry for the total energy argument.

difficult to produce a shock wave until the density behind the previous one has sufficiently decreased. This would also explain the quasiperiodicity.

As mentioned in the Introduction, density waves have been previously observed by Baxter *et al.* in a wide-angle (20°–60°) hopper filled with sand [12]. Since, as our experiment shows, the dynamics strongly depend on the angle, they may be observing a different process altogether, possibly connected with the dilatant fluctuations we see at our largest funnel angles. Their much lower wave speeds (about -2 to $+2$ cm/s depending on the hopper angle) also suggest this.

E. Other geometries

Measurements were made using geometries other than the one presented here. An early model with a sharp transition from the funnel to the reservoir always jammed permanently if β were too small, necessitating the curved transition shown in Fig. 2. A flow between two semicircles of radius 25 cm was also studied, being the simplest possible curved constriction. The power spectra in this case were completely white, aside from short-range correlations, since shock waves cannot form in such a short space.

IV. FLOW RATE MEASUREMENTS

A simple but instructive total energy argument has been given by Brown [28] to compute the flow rate. We briefly review it here with some slight alterations. The geometry is shown in Fig. 9 and applies to flow in both two and three dimensions. First, consider the total energy E of a ball of mass m and radius a rolling (without slipping) with velocity v. If we modify Brown's work by including the rotational energy, this can be written as $E=1/2\kappa mv^2+mgr\cos\phi$ where $\kappa=1+I/ma^2$ and $I=3/5ma^2$ is the moment of inertia, hence $\kappa=8/5$. (In two dimensions, where the balls roll down an inclined plane, we also have $g\rightarrow g\sin\theta$.) Then, the energy per unit mass ϵ is

$$\epsilon=\frac{1}{2}\kappa v^2+gr\cos\phi. \tag{1}$$

The granular material is now considered to be an incompressible fluid, which is only a valid assumption in the steady flow regime. Since only gravity acts on the flow, the pressure being constant (see Sec. I), Eq. (1) applies to a fluid as well. Furthermore, if the velocity field has only a radial compo-

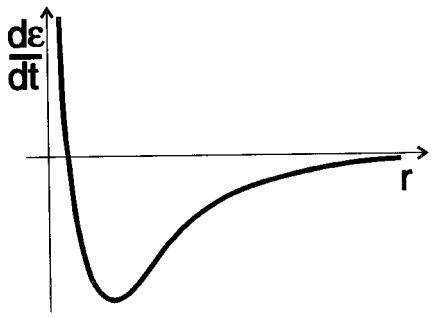

FIG. 10. A schematic of the total time derivative of the energy per unit mass.

nent, then conservation of mass requires that $v(r,\phi)=-\lambda(\phi)/r^{d-1}$ where d is the dimension of the system and $\lambda(\phi)$ is a function of the polar angle ϕ only. Substituting this into Eq. (1), we can compute the total time derivative of ϵ:

$$\frac{d\epsilon}{dt}=v\frac{\partial\epsilon}{\partial r}=v\left[-\kappa(d-1)\frac{\lambda^2(\phi)}{r^{2d-1}}+g\cos\phi\right], \tag{2}$$

which is shown schematically in Fig. 10 as a function of r.

Brown then postulated that energy can only be dissipated in the flow. Hence the radius at which $d\epsilon/dt$ switches sign (the minimum in the energy) must correspond to the radius of the outlet $R_0=D/2\sin\beta$ where the balls leave the funnel and roll freely (i.e., without dissipative interactions). [Since we are always below the angle of approach, we will ignore the statistically empty space correction (see Sec. III).] This condition at $d\epsilon/dt=0$ yields

$$\lambda=\left[\frac{g}{\kappa(d-1)}\right]^{1/2}R_0^{d-1/2}\cos^{1/2}\phi. \tag{3}$$

The volume flow rate is $Q_V=\int v(r,\phi)dA$, which for small β (so there is no stagnant region) and small θ (if $d=2$) yields the simple result

$$Q_V\cong\frac{1}{\sqrt{2}}\kappa^{-1/2}g^{1/2}D^{3/2}\beta^{-1/2}\theta^{1/2}\quad(d=2), \tag{4a}$$

$$Q_V\cong\frac{\pi}{8}\kappa^{-1/2}g^{1/2}D^{5/2}\beta^{-1/2}\quad(d=3). \tag{4b}$$

Note that the exponent for β does not depend on the dimension.

The number flow rate, which we actually measure, is then $Q=nQ_V$ where n is the mean number density and can be written as $n=C/V_d$ where C is the packing fraction and V_d is the volume of a ball (i.e., the projected area if $d=2$). Thus the flow rate in our experiment ($d=2$) in the steady flow regime is predicted to be

$$Q=\frac{\sqrt{5}}{4}\frac{C}{\pi a^2}g^{1/2}D^{3/2}\beta^{-1/2}\theta^{1/2}. \tag{5}$$

The packing fraction C is the only unknown quantity.

The average flow rate was measured by simply counting the number of balls that left the system in a given amount of time. After a short transient time, the flow quickly reached steady state, although there could be large fluctuations. For typical runs of 2–3 min, the error was $\sim 1\%$ for the steady flow regime, and as large as $\sim 10\%$ in the intermittent regime where the flow visibly fluctuated the most. We will now examine the flow rate as a function of the three flow parameters discussed in Sec. II.

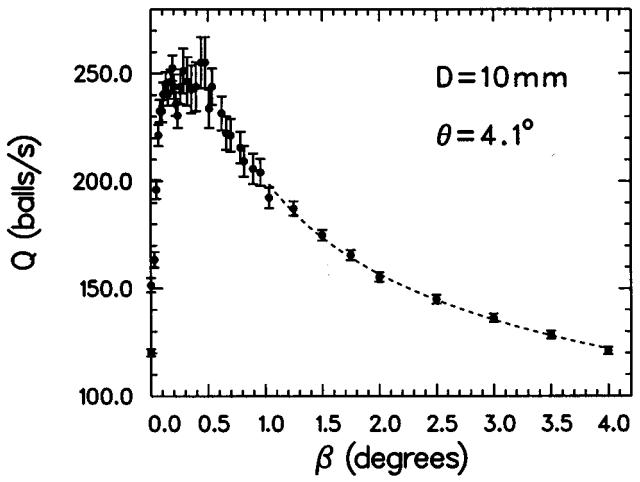

FIG. 11. The average flow rate as a function of the opening angle. The dashed line is a power-law fit (see text).

A. Opening angle β

Figure 11 shows a measurement of the average flow rate Q as a function of β with the same configuration described in Sec. III, i.e., $D=10$ mm and $\theta=4.1°$. Unexpectedly, the flow rate had a maximum at $\beta\sim 0.5°$ which is in the intermittent flow regime. The steady flow regime is to the right of the peak and the pipe flow regime to the left. The dashed line in the steady flow regime is a power-law fit yielding $Q\sim\beta^{-0.4}$, which differs slightly from the predicted value given by Eq. (5), although it is probably necessary to measure at larger β to avoid the peak. The fit also yields a packing fraction $C=0.45$ which is lower than one would expect from the nearly close packed structure observed in Fig. 3(a). This is probably because the flow rate is actually determined by the geometry at the outlet where, due to dilatancy, the density is lower than it is upstream. [We are aware that this power-law fit, and those presented later, only cover a small range of parameter values, but the general consistency with Eq. (5) is at least strongly indicative of its validity in the steady flow regime.]

The flow rate was also measured with $D=15$ and $D=25$ mm. All three measurements are shown in Fig. 12. The flow rate has been rescaled by a factor $(D/D_0)^{3/2}$ where $D_0=10$ mm (so that the data shown in Fig. 11 remain unchanged). As predicted by Eq. (5), all three measurements converge in the steady flow regime at large β. It also appears that they approach the same value at $\beta=0$, suggesting that $Q\sim D^{3/2}$ in the pipe flow regime also. Each also has a peak, always in the intermittent flow regime. However, the peak positions and amplitudes are clearly different for the different configurations. In fact, it appears that the peak position $\beta_p\approx cD/L$, where L is the length of the funnel and c is a

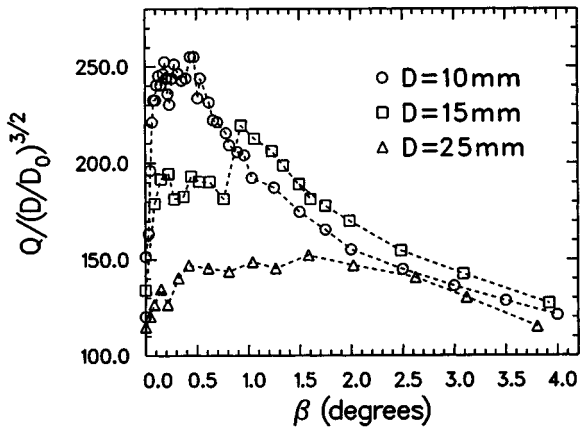

FIG. 12. The average flow rate for three different outlet widths. The flow rate has been rescaled with $D_0 = 10$ mm (see text). The dashed lines are a guide to the eye.

number of the order of unity. This suggests that the funnel length plays an important role in the intermittent flow regime although we did not test this explicitly. It is, in effect, a finite size cutoff for the validity of Eq. (5), i.e., where the flow crosses over from steady to intermittent flow. (We also pointed out in Sec. III C that pipe flow seems to occur for $\beta < a/L$.)

Let us consider Fig. 11 again. If we extrapolate the prediction of Eq. (5) to the peak, we can use our hypothesis for the peak position to arrive at an expression for the peak flow rate, namely, $Q(\beta_p) \sim DL^{1/2}$. (Of course, at sufficiently large flow rates, the assumptions leading to this result must break down otherwise the flow rate would increase without bound as $L \to \infty$.) Thus if we plot Q/D vs β/D the data shown in Fig. 12 should collapse except in the pipe flow regime near $\beta = 0$. This appears to be the case, as shown in Fig. 13.

Although Eq. (5) appears to fail in the intermittent and pipe flow regimes, we can, nevertheless, use it to explain the presence of a peak in the flow rate. Since the flow in the pipe flow regime is, in fact, steady *at the inlet*, we can still use Eq. (5) if we consider an effective opening angle $\beta^*(\beta)$ and outlet width $D^*(\beta)$ determined by the geometry at the point

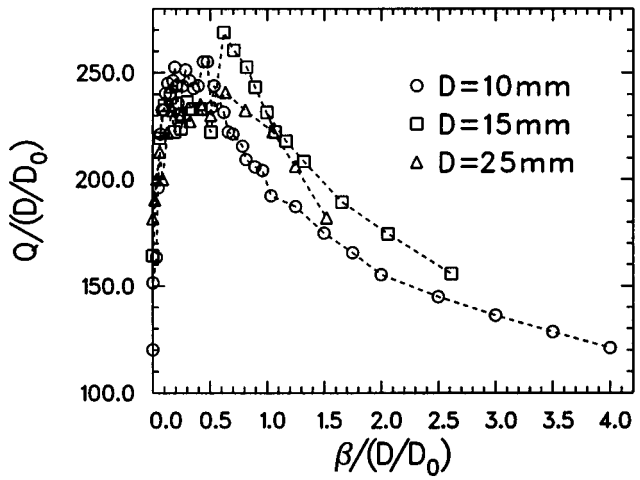

FIG. 13. Rescaled Q vs rescaled β with $D_0 = 10$ mm (see text). The dashed lines are a guide to the eye.

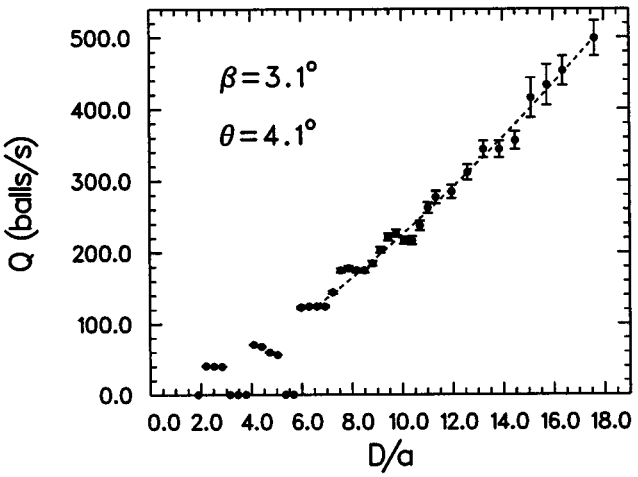

FIG. 14. The average flow rate as a function of the outlet width. The dashed line is a power-law fit (see text).

which actually controls the flow rate. Recall that in describing the general behavior of the system in Sec. III, we noted that the point which determines the flow rate moves from the outlet to the inlet as β is decreased. Thus, for steady flow, obviously $\beta^* = \beta$ and $D^* = D$. As β (and hence β^*) is decreased, the flow rate increases following Eq. (5). We then cross over to the intermittent flow regime (at a point determined by the length of the funnel) and eventually to the pipe flow regime where the flow rate becomes sensitive to the geometry at the inlet. Here, as illustrated in Fig. 2, β^* becomes rapidly larger than β, and the flow rate now decreases. During the cross over, D^* only becomes slightly larger than D so this scenario also explains the observed dependence of the flow rate on D at $\beta = 0$ since it predicts that $Q(\beta = 0) \sim D^{3/2}[\beta^*(0)]^{-1/2}$. From Fig. 11 we see that $\beta^*(0) \sim 4°$.

B. Outlet width *D*

Figure 14 shows the average flow rate Q as a function of D/a with fixed $\beta = 3.1°$ (i.e., steady flow) and $\theta = 4.1°$. It will be noted that there are discrete jumps in the flow rate.

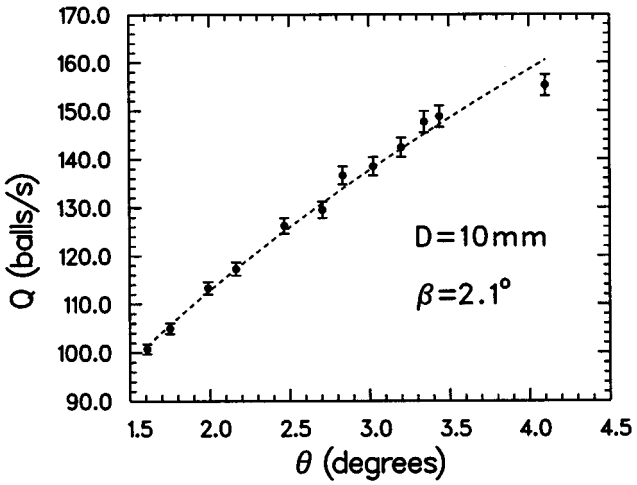

FIG. 15. The average flow rate as a function of the inclination angle. The dashed line is a power-law fit (see text).

There is obviously no flow when $D/a<2$. When $3\lesssim D/a\lesssim 4$, stable arches form in the outlet causing permanent jams and the flow stops. This happens again when $5\lesssim D/a\lesssim 6$. At other values of D/a, the flow does not jam (even for sufficiently long runs) although a steplike structure is still discernible in the data for $D/a>6$. The dashed line is a power-law fit which yields $Q\sim D^{1.4}$, in reasonable agreement with Eq. (5). The packing fraction is $C=0.51$, again lower than expected, but consistent with the value found in the preceding section.

C. Inclination angle θ

Figure 15 shows the average flow rate Q as a function of θ with fixed $\beta=2.1°$ (steady flow) and $D=10$ mm. For $\theta\lesssim 0.7°$, the balls will not roll. The dashed line is a power-law fit which yields $Q\sim\theta^{0.5}$ in agreement with Eq. (5) and a packing fraction $C=0.53$ which is consistent with the previous sections.

V. SUMMARY

We have presented the results of measurements of a granular flow in a two dimensional funnel. The behavior of the flow can be controlled by the opening angle β. At rather small angles, the flow has different flow regimes. For $\beta>2°$ we find a steady flow with weak dilatant fluctuations. In this case, the flow rate is determined by the geometry at the outlet. When $0.1°\lesssim\beta\lesssim 1°$, the flow exhibits large density fluctuations in the form of quasiperiodic kinematic shock waves. The flow rate is a maximum in this regime. When $\beta\lesssim 0.05°$, the shock waves become stationary and the flow rate is determined by the geometry at the inlet which actually causes it to decrease. For all the flow regimes, the power spectra of the number density fluctuations were white at low frequencies.

ACKNOWLEDGMENTS

It is a pleasure to thank G. Grinstein, A.M. Hansen, H.J. Herrmann, A. Johansen, K. Måløy, S.R. Nagel, G. Peng, V. Putkaradze, and S. Schwarzer for many illuminating discussions. We especially appreciate the efforts of S. Hørlück, who constructed the video system. The authors would also like to thank the Danish Science Foundation (Statens Naturvidenskabelige Forskningsråd) and Novos Fond for support.

[1] R.L. Brown and J.C. Richards, *Principles of Powder Mechanics* (Pergamon Press, Oxford, 1970).
[2] S.B. Savage, Adv. Appl. Mech. **24**, 289 (1984).
[3] C.S. Campbell, Annu. Rev. Fluid Mech. **22**, 57 (1990).
[4] H.M. Jaeger and S.R. Nagel, Science **255**, 1523 (1992).
[5] *Disorder and Granular Media*, edited by D. Bideau and A. Hansen (North-Holland, Amsterdam, 1993).
[6] *Mobile Particulate Systems*, Vol. 287 of *NATO Advanced Study Institute, Series E: Applied Sciences*, edited by E. Guazzelli and L. Oger (Kluwer, Dordrecht, 1995).
[7] H. Hayakawa, H. Nishimori, S. Sasa, and Y-h. Taguchi, Jpn. J. Appl. Phys. **34**, 397 (1995).
[8] G. Hagen, Berl. Monatsb. Akad. Wiss. 35 (1852); H.A. Janssen, Z. Ver. Dtsch. Ing. **39**, 1045 (1895).
[9] C.T. Veje, Master's thesis, University of Copenhagen, 1995.
[10] See, for example, M.F. Handley and M.G. Perry, Powder Technol. **1**, 245 (1967); V.L. Rao and D. Venkateswarlu, *ibid.* **11**, 133 (1975); M.G. Perry and H.A.S. Jangda, *ibid.* **4**, 89 (1970); S.B. Savage, J. Fluid Mech. **92**, 53 (1979).
[11] See, for example, J.O. Cutress and R.F. Pulfer, Powder Tech. **1**, 213 (1967); R.L. Michalowski, *ibid.* **39**, 29 (1984); T.G. Drake, J. Geophys. Res. **95**, 8681 (1990).
[12] G.W. Baxter, R.P. Behringer, T. Fagert, and G.A. Johnson, Phys. Rev. Lett. **62**, 2825 (1989).
[13] K.L. Schick and A.A. Verveen, Nature (London) **251**, 599 (1974).
[14] C.T. Veje and P. Dimon (unpublished).
[15] X. Wu, K.J. Måløy, A. Hansen, M. Ammi, and D. Bideau, Phys. Rev. Lett. **71**, 1363 (1993).
[16] P.K. Haff, J. Fluid Mech. **134**, 401 (1983).
[17] C. Brennen and J.C. Pearce, J. Appl. Mech. **45**, 43 (1978).
[18] S.B. Savage and D.J. Jeffrey, J. Fluid Mech. **110**, 255 (1981).
[19] A. Mehta and S.F. Edwards, Physica A **157**, 1091 (1989).
[20] J. Lee, Phys. Rev. E **49**, 281 (1994).
[21] G.H. Ristow and H.J. Herrmann, Phys. Rev. E **50**, 5 (1994).
[22] G. Peng and H.J. Herrmann, Phys. Rev. E **49**, 1796 (1994); **51**, 1745 (1995).
[23] G.W. Baxter and R.P. Behringer, Phys. Rev. A **42**, 1017 (1990).
[24] S. Schwarzer (private communication).
[25] M. van Dyke, *An Album of Fluid Motion* (The Parabolic Press, Stanford, 1988).
[26] O. Reynolds, Philos. Mag. S. **20**, 469 (1885).
[27] See, for example, G. B. Whitham, *Linear and Nonlinear Waves* (Wiley, New York, 1974).
[28] R.L. Brown, Nature (London) **191**, 458 (1961). See also [1].